

# LOCAL BUCKLING OF COLD-FORMED STAINLESS STEEL SECTIONS

K J R Rasmussen

Department of Civil Engineering, University of Sydney

T Burns

Department of Civil Engineering, University of Sydney

P Bezkorovainy

Department of Civil Engineering, University of Sydney

M R Bambach

Department of Civil Engineering, University of Sydney

Copyright © 2003 The Steel Construction Institute

## Abstract

*Research at the University of Sydney, in the stainless steel area has for the last three years concentrated on the local buckling strength of stainless steel plates with application to cold-formed sections. The research has encompassed tests on single stainless steel plates, and the finite element modelling of stainless steel plates. Research was also carried out to determine the stress-strain curves for stainless steel materials over the full strain range solely in terms of the Ramberg-Osgood parameters ( $n$ ,  $\sigma_{0.2}$ ,  $E_0$ ). Advanced finite element models have been used to derive direct expressions for the plate strength in terms of the Ramberg-Osgood parameters using a modified Winter curve. The explicit plate strength equations showed that as a result of gradual yielding, the strength of stainless steel plates is reduced below the strength of carbon steel plates, as predicted by the standard Winter equation, by up to 13% depending on the alloy and cold-working history. Most recently, the explicit strength equations were applied to cold-formed sections and design models were proposed for determining the strength of such sections. It was shown that the corners of cold-formed sections play a more important role for stainless steel sections than for carbon steel sections because the corner areas can be cold-worked to much higher strengths than in the case of carbon steel sections. Because of the enhanced mechanical properties of the corners, the standard Winter equation can in many cases be used safely for the design of cold-formed stainless steel sections. There are however a number of exceptions, which have been identified. The present paper summarises the research on the local buckling strength conducted at the University of Sydney over the last three years.*

## 1 INTRODUCTION

Early research on inelastic buckling embraced the use of moduli to account for the loss of stiffness associated with non-linear stress-strain curves [1]. With application mainly to aluminium structures, the tangent modulus ( $E_t$ ) was shown to be applicable to columns failing by flexural buckling [1], and later to stainless steel columns [2]. The first specification for cold-formed stainless steel structural members [3] adopted the use of the tangent modulus in its compression member provisions, and the same provisions have been used since, including in the most recent edition of the specification, now in limit states format [4].

Stowell's classic work [5] on the inelastic buckling of plates demonstrated that the plate strength is also affected by gradual material yielding. Bleich [1] reworked Stowell's plate buckling differential equation and showed that the inelastic strength of plates supported along both longitudinal edges (stiffened plates) can be obtained by substituting the combined modulus  $\sqrt{E_0 E_t}$  in place of the initial modulus  $E_0$  in the elastic plate buckling equation. Since  $\sqrt{E_0 E_t} < E_t$ , it could be concluded that the buckling of plates is less affected by gradual yielding than columns.

Johnson and Winter [2] and Wang et al. [6] conducted compression and bending tests on annealed and cold-reduced AISI304 hat sections with slender stiffened flanges and concluded that the same Winter equation as obtained for carbon steel sections could also be used for the stainless steel stiffened elements. While this result was at odds with classical theory, which would suggest the use of a reduction factor (often

referred to as a plasticity reduction factor), it formed the basis for the American [3, 4] and Australian [7] provisions for stiffened and unstiffened elements of cold-formed stainless steel structural elements. However, the result has been challenged by van den Berg [8] who provided test results showing that the standard Winter equation (1),

$$\chi_w = \begin{cases} 1 & \text{for } \lambda \leq 0.673 \\ 1/\lambda - 0.22/\lambda^2 & \text{for } \lambda > 0.673 \end{cases} \quad (1)$$

$$\lambda = \sqrt{\frac{\sigma_{0.2}}{\sigma_{cr}}} \quad (2)$$

$$\sigma_{cr} = \frac{k\pi^2 E_0}{12(1-\nu^2)} \left(\frac{t}{b}\right)^2 \quad (3)$$

may lead to unsafe design strength prediction. In eqn. (3),  $E_0$  is the *initial* elastic modulus,  $t$  and  $b$  are the plate thickness and width respectively, and  $k$  is the plate buckling coefficient, which is to be taken as 4 and 0.5 for stiffened and unstiffened plates respectively according to the American and Australian standards.

The contradicting literature on the local buckling strength of cold-formed stainless steel sections combined with the inconsistency between classical inelastic plate buckling theory and current design provisions triggered the research described in the present paper. The objective of this research was to investigate the validity of current design recommendations for stiffened elements in cold-formed sections and to propose remedies for sections that might not be safely designed according to current provisions.

The approach taken in the work presented herein follows research on the strength of stainless steel columns, as reported in [9, 10]. One of the main goals was to derive direct expressions for the plate strength in terms of the parameters describing the stress-strain curve, here chosen as the Ramberg-Osgood parameters. With these expressions at hand, design curves can be obtained for representative groups of stainless steel alloys, as will be presented. However, as will also be shown, corners may contribute significantly to the strength of cold-formed sections because of their enhanced mechanical properties. In fact, the enhanced corner properties may offset the reduction in strength caused by gradual yielding.

## 2 TESTS OF SINGLE PLATES

### 2.1 Plate tests

Two tests were conducted on single plates cut from nominally 3 mm thick UNS31803 stainless steel plate, popularly known as Duplex 2205. The nominal widths were chosen as 125 mm and 250 mm, which corresponded to plate slenderness values ( $\lambda = \sqrt{\sigma_y/\sigma_{cr}}$ ) of 1.03 and 2.06 respectively when using nominal values of yield stress and initial Young's modulus of 440 MPa and 200,000 MPa respectively. The nominal length of the plates was 750 mm which produced aspect ratios of 6 and 3 for the 125 mm and 250 mm wide plates respectively. The plates were guillotined to size. They were simply supported along all four edges in the test rig. Figure 1 shows a photo of the test of the 250 mm wide plate at advanced stages of loading. Further details of the tests are given in [11].

The plate test rig used the "finger principle" developed at Cambridge University to a) provide simple supports at the longitudinal supports and b) ensure that the axial thrust was not transferred to the longitudinal supports. Bearings were used at the loaded ends to allow flexural rotations. The plates were subjected to uniform compression and tested under stroke control until failure. Full details of the rig are given in [12].

The test specimens were comprehensively instrumented to allow detailed comparison between experimental and numerical load vs displacement and load vs strain responses. A displacement transducer frame was placed over the rig to measure the deflection along the centre of the plate. A transducer was mounted on a plate sliding along linear bearings so that by taking frequent readings the longitudinal profile

of the plate deflection could be obtained. The deflections were also measured prior to the test to obtain the initial out-of-flatness.

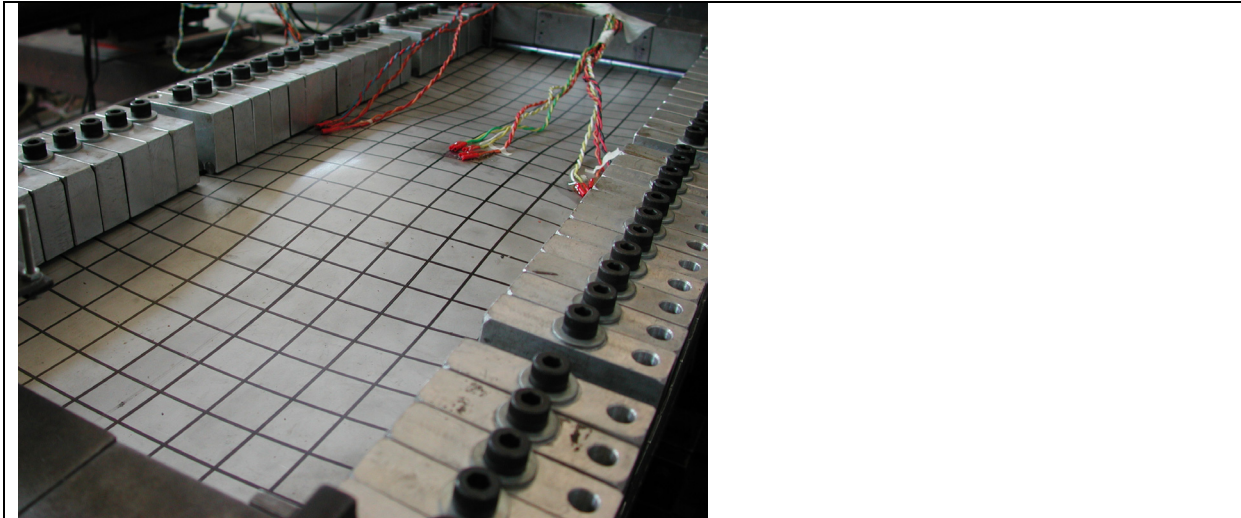


**Figure 1** Test of stainless steel single plate

## 2.2 Material tests

The material properties of the stainless steel alloy S31803 were obtained from coupon tests of small sample plates cut from the same larger plates as those used for the plate test specimens. Tension and compression coupons were cut from each sample plate in the longitudinal, transverse and diagonal directions so as to obtain data for the anisotropic properties of the material. The full set of stress-strain curves are shown in [11].

The mechanical properties are summarised in Table 1. They include the initial elastic modulus ( $E_0$ ), the ultimate tensile strength ( $\sigma_u$ ), and the Ramberg-Osgood parameter ( $n$ ) calculated as,

$$n = \frac{\ln(20)}{\ln(\sigma_{0.2} / \sigma_{0.01})} \quad (4)$$

where  $\sigma_{0.01}$  and  $\sigma_{0.2}$  are the 0.01% and 0.2% proof stresses respectively.

**Table 1** Mechanical properties of S31803 alloy obtained from coupon test data

Specimen	$E_0$ (MPa)	$\sigma_{0.01}$ (MPa)	$\sigma_{0.2}$ (MPa)	$\sigma_{ult}$ (MPa)	$n$
TT	215250	430	635	831	7.7
LT	200000	310	575	740	4.8
DT	195000	376	565	698	7.4
TC	210000	380	617	-	6.2
LC	181650	275	527	-	4.6
DC	205000	460	610	-	10.6

## 3 NUMERICAL MODELLING

### 3.1 General

It is well known that stainless steel alloys have different properties in compression and tension and different properties in the transverse and longitudinal directions, particularly when subjected to cold-working, eg. by cold-reducing the thickness or cold-rolling sheet or coil into structural shapes. These characteristics require careful material modelling particularly in the case of plated structures in compression which develop two-dimensional stress states during buckling.

In numerical analyses, the modelling of nonlinear stress-strain curves is straightforward in most finite element packages. However, these material models assume *isotropic* nonlinear hardening and as such cannot model stainless steel alloys accurately. Abaqus includes a facility for modelling anisotropy based on Hill's theory [13], which was used in [11] to ascertain the importance of modelling anisotropy in the advanced nonlinear analysis of stainless steel plates. The study was only indicative, however, since Hill's anisotropic theory assumes elastic-perfectly-plastic material behaviour and does not account for strain hardening.

### 3.2 Numerical models

Several numerical models were tried out using isotropic and anisotropic material models as well as different models for the geometric imperfection, as described in detail in [11]. The material parameters defining the Hill's yield surface were determined on the basis of the longitudinal, transverse and diagonal compression coupon tests. The isotropic material model was based on the stress-strain curve obtained from the compression coupon test corresponding to the longitudinal direction.

Figure 2 shows a typical comparison between the experimental test and numerical load versus axial shortening graphs. The labels shown in Fig. 2 refer to the models defined in Table 2.

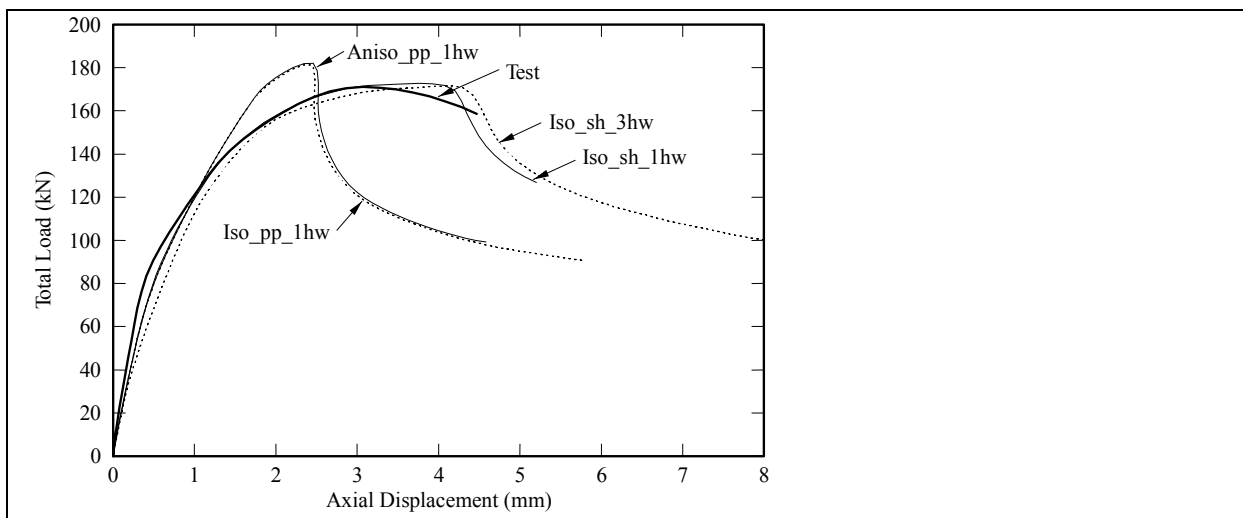


**Figure 2** Load versus axial displacement graphs

**Table 2** Ultimate loads for 250 mm wide plate

Model	Imperfection Type	Material Type	Ult. Load (kN)	Error* (%)
Iso-sh-3hw	3 symm. Half-waves <sup>#</sup>	Isotropic strain hardening	171.2	0.4
Iso-sh-1hw	1 asymm. Half-wave <sup>\$</sup>	Isotropic strain hardening	172.4	1.1
Iso-pp-1hw	1 asymm. Half-wave <sup>\$</sup>	Isotropic perfect plasticity	179.9	5.5
Aniso-pp-1hw	1 asymm. Half-wave <sup>\$</sup>	Anisotropic perfect plasticity	181.2	6.3

\* Relative to test value,  $P_u=170.5$  kN

# Elastic buckling mode scaled to measured imperfection magnitude

\$ As measured

The conclusions of the study were that:

- Excellent agreement with tests can be achieved by using the stress-strain curve for longitudinal compression, assuming isotropic hardening, and modelling the as-measured geometric imperfection (model Iso\_sh\_1hw). The ultimate load obtained using this model was 3.6% less and 1.1% more than the experimental ultimate loads for 125 mm and 250 mm wide test plates respectively. When modelling the geometric imperfection by scaling the elastic local buckling mode rather than using the measured values, the numerical ultimate loads differed by 3.8% in the case of the relatively stocky 125mm wide plate, whereas the ultimate loads differed by just 0.7% in the case of the relatively slender 250mm wide plate. Hence, the modelling of the geometric imperfection (magnitude and shape) is mainly important for relatively stocky plates ( $\lambda \cong 1$ ).

- The modelling of anisotropy may not be important for stainless steel plates. The measured values of 0.2% proof stress (compression) for the longitudinal and transverse directions differed by 17%, yet the ultimate loads differed by up to just 0.8%. However, this conclusion was drawn on the basis of Hill's theory assuming elastic-perfectly-plastic material behaviour. The effect of anisotropy may be more pronounced in a strain hardening model where anisotropy plays a role at significantly lower stresses than in elastic-perfectly-plastic models.

#### 4 FULL-RANGE STRESS-STRAIN CURVES

The isotropic material nonlinear finite element model developed as part of the numerical study was used for generating plate strength curves for sets of Ramberg-Osgood parameters ( $E_0, \sigma_{0.2}, n$ ). Initially, stress-strain curves were generated for various values of  $n$  and non-dimensional proof stress ( $e$ ),

$$e = \frac{\sigma_{0.2}}{E_0} \tag{5}$$

using the standard Ramberg-Osgood expression,

$$\varepsilon = \frac{\sigma}{E_0} + 0.002 \left( \frac{\sigma}{\sigma_{0.2}} \right)^n \tag{6}$$

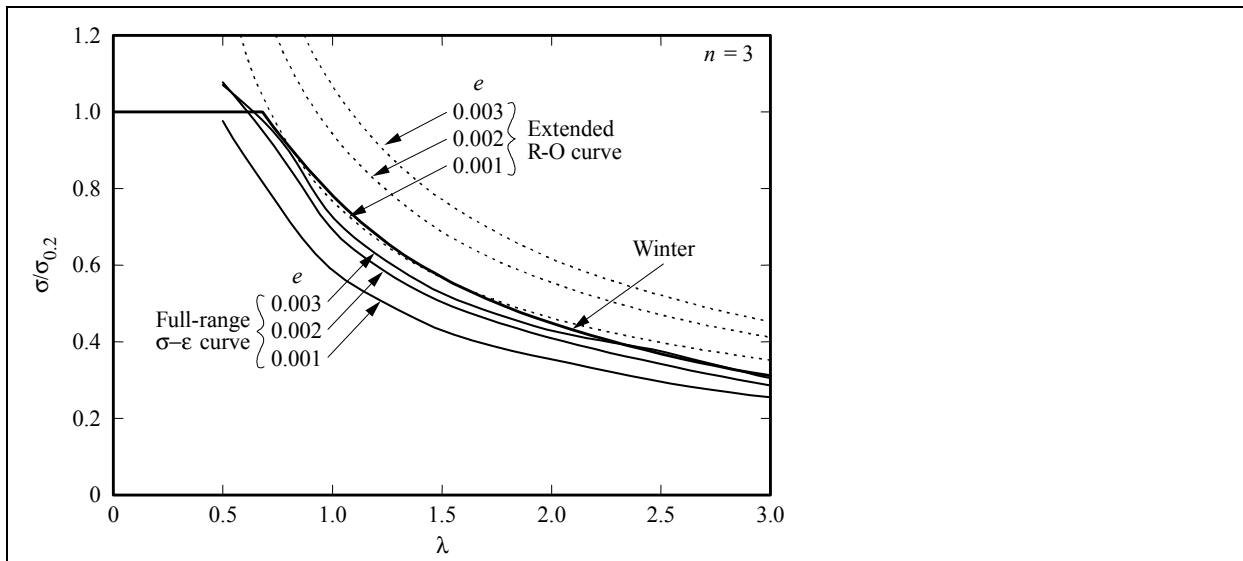


**Figure 3** Plate strength curves for different material models

To cover the strain values reached in the numerical analyses, the Ramberg-Osgood stress-strain curve was extended well beyond the 0.2% proof stress ( $\sigma_{0.2}$ ). Extending the stress-strain curve past the 0.2% proof stress produced plate strength curves which were evidently erroneous, as shown in Fig. 3. On examining the stresses reached in the analysis, it became apparent that when the  $n$ -parameter is determined to fit the initial part of the stress-strain curve, eg. by using eqn. (4), the standard Ramberg-Osgood equation (6) is likely to significantly overestimate the actual stress-strain curve then extended beyond the 0.2% proof stress. A similar observation has also been made in [14]. In response, research was carried out to derive expressions that would allow the stress-strain curve to be determined accurately over the full range of strain values, as described in [15]. The objective was to be able to define the full-range curve in terms of the Ramberg-Osgood parameters ( $E_0, \sigma_{0.2}, n$ ), as determined for the initial part of the stress-strain curve.

The following expression was proposed for the full-range engineering stress-strain curve,

$$\varepsilon = \begin{cases} \frac{\sigma}{E_0} + 0.002 \left( \frac{\sigma}{\sigma_{0.2}} \right)^n & \text{for } \sigma \leq \sigma_{0.2} \\ \frac{\sigma - \sigma_{0.2}}{E_{0.2}} + \varepsilon_u \left( \frac{\sigma - \sigma_{0.2}}{\sigma_u - \sigma_{0.2}} \right)^m + \varepsilon_{0.2} & \text{for } \sigma > \sigma_{0.2} \end{cases} \quad (7)$$

where  $\varepsilon_u$  is the engineering strain corresponding to the engineering ultimate tensile strength ( $\sigma_u$ ), and  $\varepsilon_{0.2}$  is strain corresponding to the 0.2% proof stress,

$$\varepsilon_{0.2} = \frac{\sigma_{0.2}}{E_0} + 0.002. \quad (8)$$

The stress-strain curve defined by eqn. (7) uses a transformed Ramberg-Osgood equation with exponent  $m$  for stresses in the range from  $\sigma_{0.2}$  to  $\sigma_u$ . A similar compound stress-strain curve had previously been proposed by Real and Mirambell [14]. The following expressions were derived for  $m$ ,  $\varepsilon_u$  and  $\sigma_u$ :

$$m = 1 + 3.5 \frac{\sigma_{0.2}}{\sigma_u} \quad (9)$$

$$\varepsilon_u = 1 - \frac{\sigma_{0.2}}{\sigma_u} \quad (10)$$

$$\frac{\sigma_{0.2}}{\sigma_u} = 0.2 + 185e \quad (\text{austenitic and duplex alloys}) \quad (11)$$

$$\frac{\sigma_{0.2}}{\sigma_u} = \frac{0.2 + 185e}{1 - 0.0375(n - 5)} \quad (\text{all alloys}). \quad (12)$$

Equation (11) was shown to accurately predict the ultimate tensile strength of austenitic and duplex alloys. It was modified in the form of eqn. (12) to also cover ferritic alloys. However, eqn. (12) is less accurate for austenitic and duplex alloys than eqn. (11), as described in [15]. Figure 4 shows a typical comparison between a measured stress-strain curve and the stress-strain curves obtained using the standard Ramberg-Osgood curve and the extended Ramberg-Osgood curve.

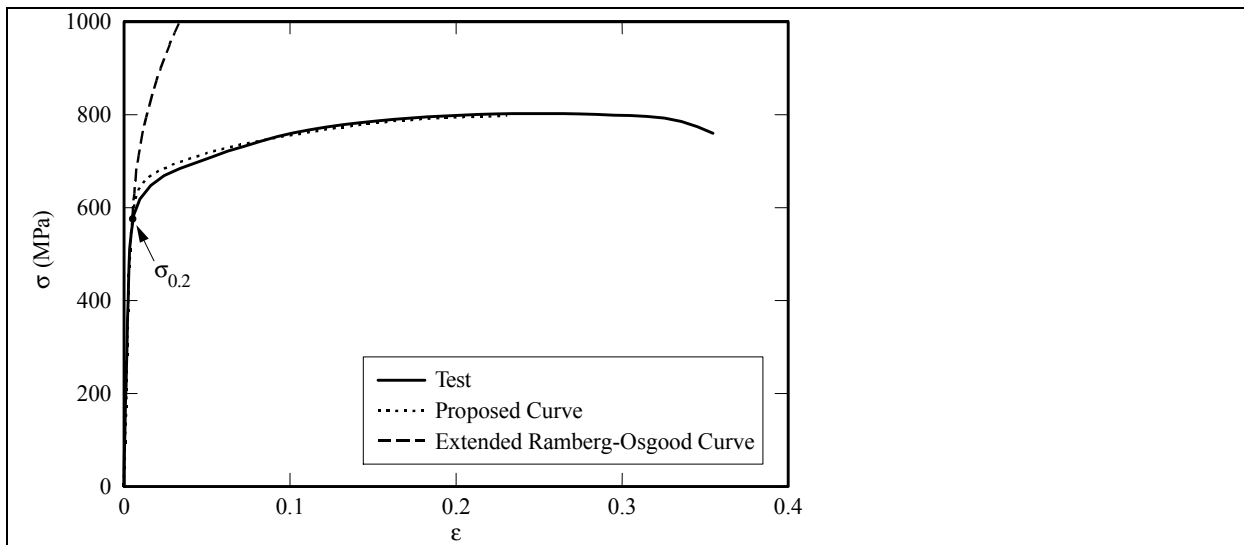


**Figure 4** Stress-strain curves for S31803 alloy [15], (LT coupon test as shown in Table 1)

## 5 PLATE STRENGTH CURVES

### 5.1 Finite element results

The full-range stress-strain curve defined by eqns (7-12) was used to generate material data for finite element analyses of stiffened plates for a range of  $e$  and  $n$ -values, as described in [16]. For each  $(e,n)$ -combination of the following values,

- $e = 0.001, 0.0015, 0.002, 0.0025, 0.003$  and
- $n = 3, 5, 10, 100,$

analyses were performed over a range of plate slenderness values ( $\lambda$ ) to allow the nondimensional plate strength curve  $s$  vs  $\lambda$  to be determined, where  $s$  is the ultimate load divided by the “squash” load ( $P_{FE,ult}/(\sigma_{0.2}bt)$ ). In the analyses, the plate width was kept constant with the thickness varying to produce the desired plate slenderness value. Based on typical measurements of geometric imperfections of thin-walled sections obtained at the University of Sydney, a geometric imperfection was included in the shape of the elastic local buckling mode, scaled to a magnitude of a tenth of the thickness. No residual stress was considered.

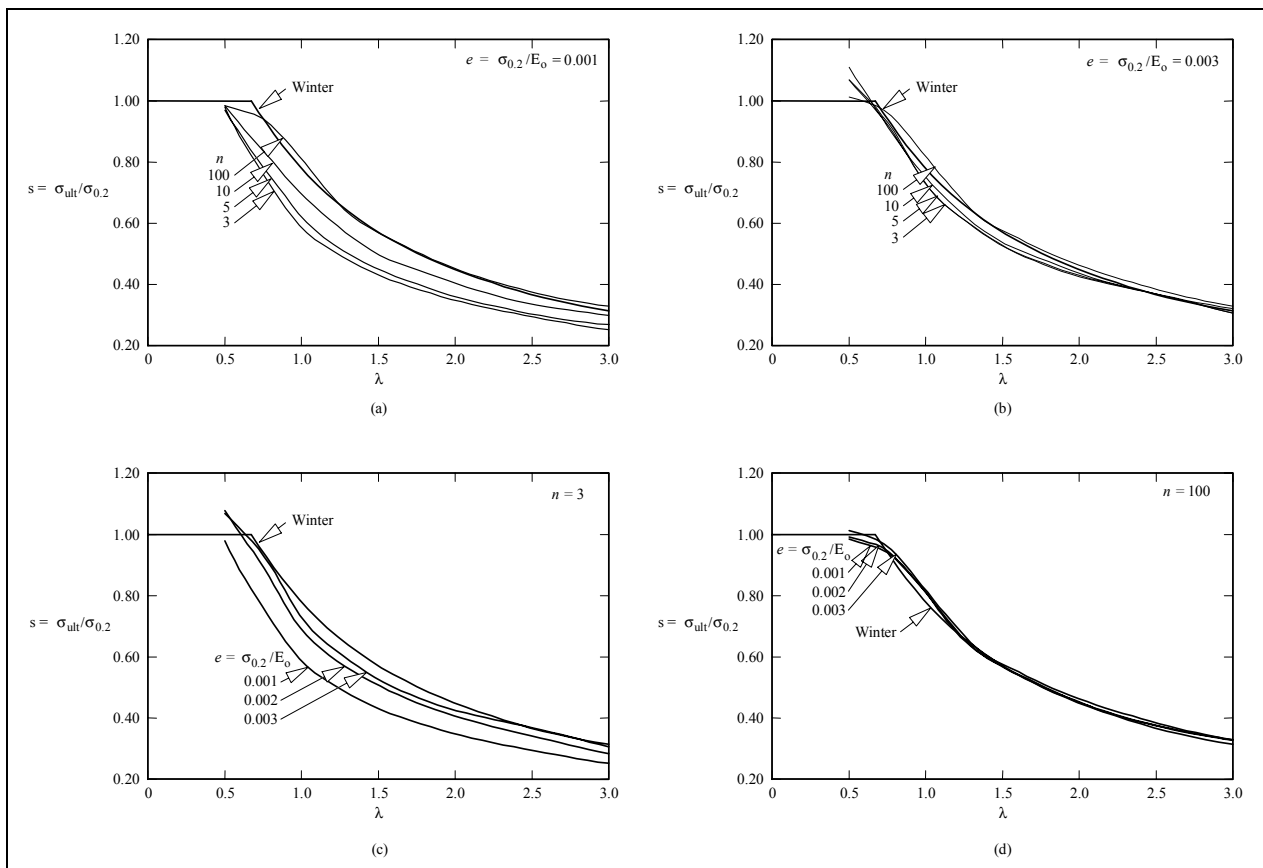


**Figure 5** Plate strength curves for stainless steel stiffened elements

Figures 5a-d show plate strength curves for various values of  $e$  and  $n$ . The figures include the Winter curve, as defined by eqn. (1), which is applicable to carbon steel plates. The curves corresponding to  $n = 100$  are representative of a bi-linear material, such as carbon steel, and are seen to be in agreement with the Winter curve. The influence of the  $n$ -parameter is demonstrated in Figure 5a for  $e = 0.001$ : Evidently, the more prominent the gradual yielding (decreasing  $n$ -value), the more the plate strength is reduced. The influence of the  $n$ -value is less, however, for plates with higher 0.2% proof stress, as shown in Fig. 5b for an  $e$ -value of 0.003, (corresponding to a proof stress of 600 MPa when assuming  $E_0=200\text{GPa}$ ). Figure 5c shows that the nondimensional plate strength is also sensitive to changes in nondimensional proof stress ( $e$ ), and that it increases with increasing proof stress. This result is in contrast to the strength of carbon steel plates which are essentially independent of the proof stress, as shown in Fig. 5d. The conclusions here drawn from Figs 5a-d are consistent with those obtained for columns [9].

## 5.2 General strength curve formulation

Having obtained plate strength curves for a wide range of  $(e,n)$ -values covering the practical range for structural stainless steel alloys, a generalised Winter equation,

$$\chi = \alpha / \lambda - \beta / \lambda^2 \quad (13)$$

was used to fit the strength curves by treating the  $\alpha$  and  $\beta$  parameters as functions of  $e$  and  $n$ . The following relationships were obtained,

$$\alpha = \begin{cases} 0.92 + 0.07 \tanh\left(\frac{n-3}{2.1}\right) - (0.026 \exp[-0.55(n-3)] + 0.019)(6 - 2000e) & 3 \leq n \leq 10 \\ \alpha_{10} + (1 - \alpha_{10}) \frac{n-10}{90} & 10 < n \leq 100 \end{cases} \quad (14)$$

$$\beta = \begin{cases} 0.18 + 0.045 \tanh\left(\frac{n-3}{2.5}\right) - (0.01 \exp[-1.6(n-3)] + 0.005)(6 - 2000e) & 3 \leq n \leq 10 \\ \beta_{10} + (0.22 - \beta_{10}) \frac{n-10}{90} & 10 < n \leq 100 \end{cases} \quad (15)$$

where  $\alpha_{10}$  and  $\beta_{10}$  are the values of  $\alpha$  and  $\beta$  calculated at  $n=10$  respectively,

$$\alpha_{10} = 0.9898 - 0.01955(6 - 2000e) \quad (16)$$

$$\beta_{10} = 0.2247 - 0.005(6 - 2000e). \quad (17)$$

The expressions (14,15) for  $\alpha$  and  $\beta$  approach the Winter values of 1 and 0.22 for  $n \rightarrow 100$ . Good agreement was achieved between finite element strength curves and fitted curves, as exemplified in Fig. 6 for  $e=0.002$ . A detailed comparison of the numerical and fitted strength curves is made in [16].

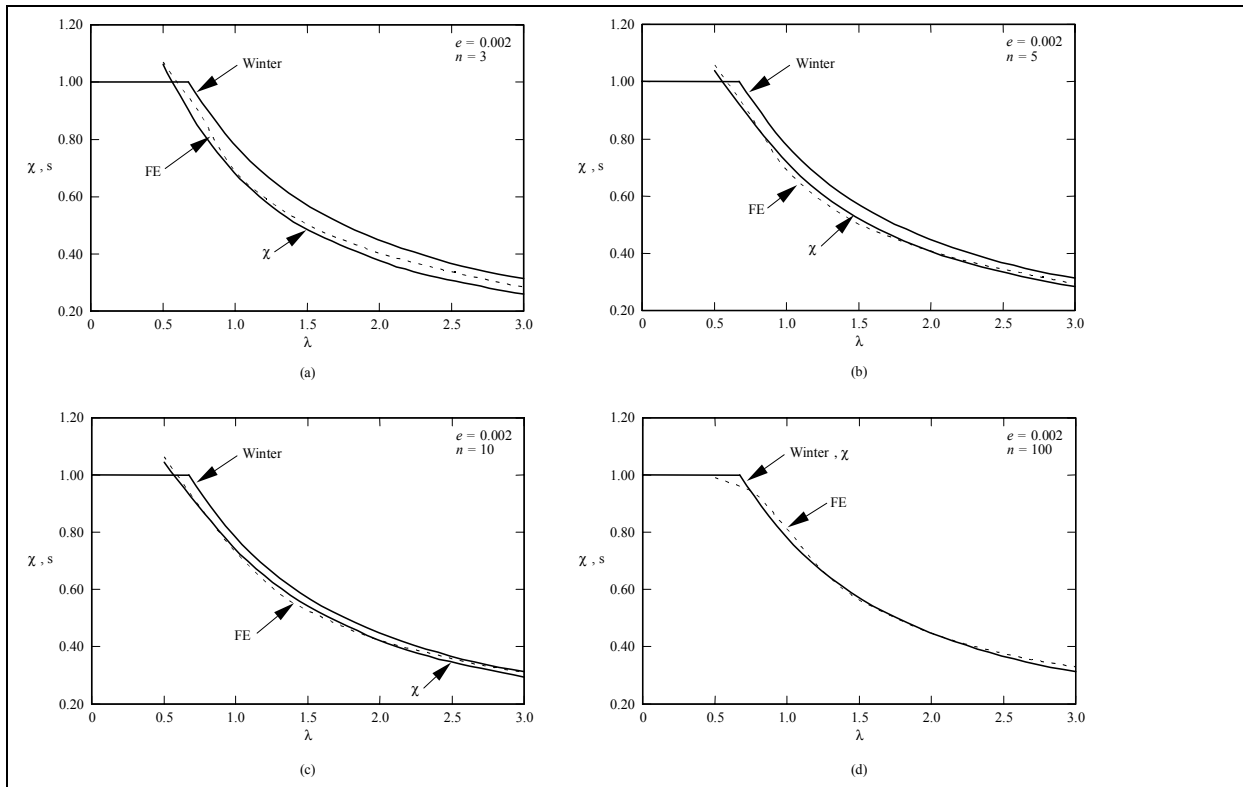


**Figure 6** Comparison between finite element and fitted plate strength curves

### 5.3 Proposed plate strength curves European approach

Part 1.4 of Eurocode3 [17] operates with strength classes and cold-worked strength grades. In a study of column strength, it was shown in [10] that while, in principle, different strength curves pertain to different alloys, the strength classes and cold-worked strength grades of Eurocode3, Part 1.4 can be divided into three distinct groups (a, b and c) with their own representative column strength curve. The groups and their representative values of Ramberg-Osgood parameters ( $E_0$ ,  $\sigma_{0.2}$ ,  $n$ ) are shown in Table 3.

**Table 3** Grouping of strength classes and cold-worked grades, and representative values of  $n$ ,  $\sigma_{0.2}$ ,  $\alpha$  and  $\beta$

Group	Plate strength curve	Alloys	Strength class/grade	$\sigma_{0.2}$ (MPa)	$n$	$e^*$	$\alpha$	$\beta$
a	a-curve	austenitic, duplex	S350, S480, C700, C850	480	4	0.022	0.91	0.19
b	b-curve	austenitic, duplex	S220, S240, S290	240	5	0.0012	0.87	0.19
c	c-curve	ferritic, 3Cr12		250	7.5	0.00125	0.91	0.21
a, b, c	Prop. Curve	all	all				0.9	0.2

\* Based on  $E_0=200$  GPa

Using the same grouping of strength classes and cold-worked strength grades for stainless steel stiffened plates, the values of  $\alpha$  and  $\beta$  corresponding to their representative Ramberg-Osgood parameters are also shown in Table 3, as obtained from [18]. The strength curves produced by these ( $\alpha$ ,  $\beta$ )-values are shown in Fig. 7. They are closely spaced and, unlike columns, can be represented by a single curve defined by  $\alpha=0.9$  and  $\beta=0.2$ , as also shown in Fig. 7. This curve is about 10% below the Winter curve.

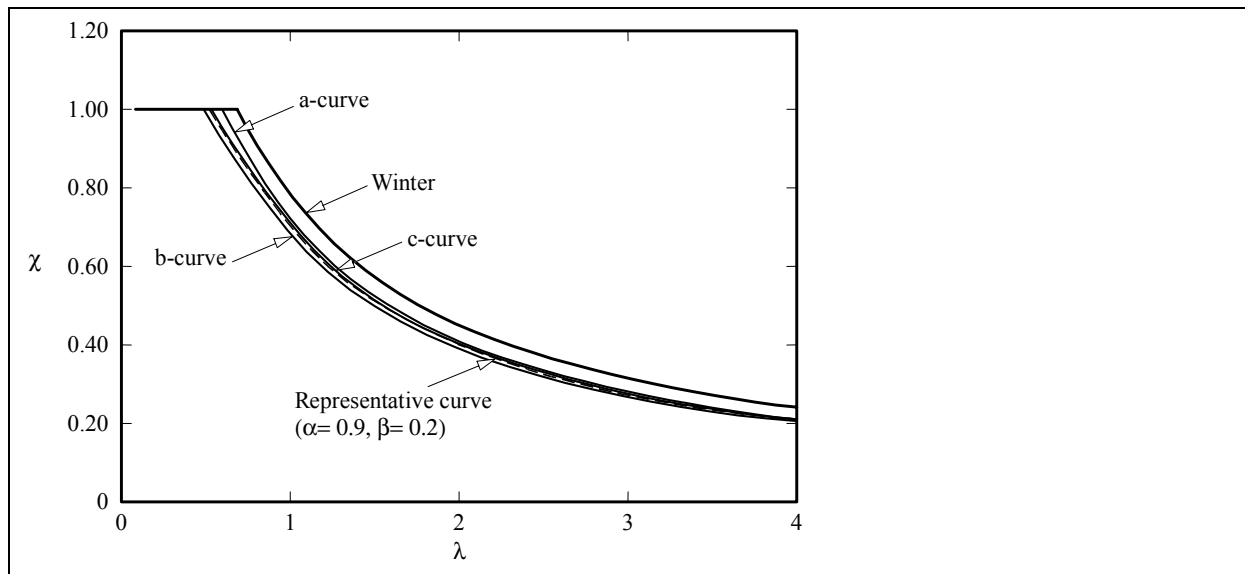


**Figure 7** Strength curves for stiffened plates using the values of ( $E_0$ ,  $\sigma_{0.2}$ ,  $n$ ) representing the a, b and c-groups of strength classes and cold-worked grades shown in Table 3.

### Australian and American approach

The Australian and American standards provide values of the Ramberg-Osgood parameters for a range of common alloys. By substituting the Ramberg-Osgood parameters pertaining to longitudinal compression into eqns (14,15), the ( $\alpha$ , $\beta$ )-values shown in Table 4 can be obtained. The corresponding plate strength curves are shown in Fig. 8.

The plate strength curves for the ferritic alloys (409, 1.4003, 430) and the duplex alloy (S31803) are closely spaced, as shown in Fig. 8, and can be represented by a Curve 1 defined by  $\alpha=0.92$  and  $\beta=0.2$ , (the mean of the ( $\alpha$ , $\beta$ )-values shown in Table 4 for these alloys). This curve matches closely the curve proposed for

the European strength classes and cold-worked strength grades. However, the strength curve for the (annealed) austenitic alloys 304(L) and 316(L) is lower, and can be represented by a Curve 2 defined by  $\alpha=0.82$  and  $\beta=0.17$ , as shown in Fig. 8. This curve is lower than that obtained for the corresponding Group b because the  $n$  and  $\sigma_{0.2}$  values specified in the Australian and American standards for these alloys are significantly lower than those given in the Eurocode3, Part 1.4.

**Table 4**  $\alpha$  and  $\beta$  values for the values of  $(E_0, \sigma_{0.2}, n)$  specified in the American and Australian standards

Alloy	$E_0$ (GPa)	$\sigma_{0.2}$ (MPa)	$n$	$e$	$\alpha$	$\beta$
304/316 and 304L/316L	195	195	4	0.00100	0.815	0.169
409	185	205	9.5	0.00111	0.915	0.206
1.4003	210	260	7.5	0.00124	0.913	0.205
430	185	275	6.5	0.00149	0.916	0.205
S31803	195	435	5	0.00223	0.929	0.202

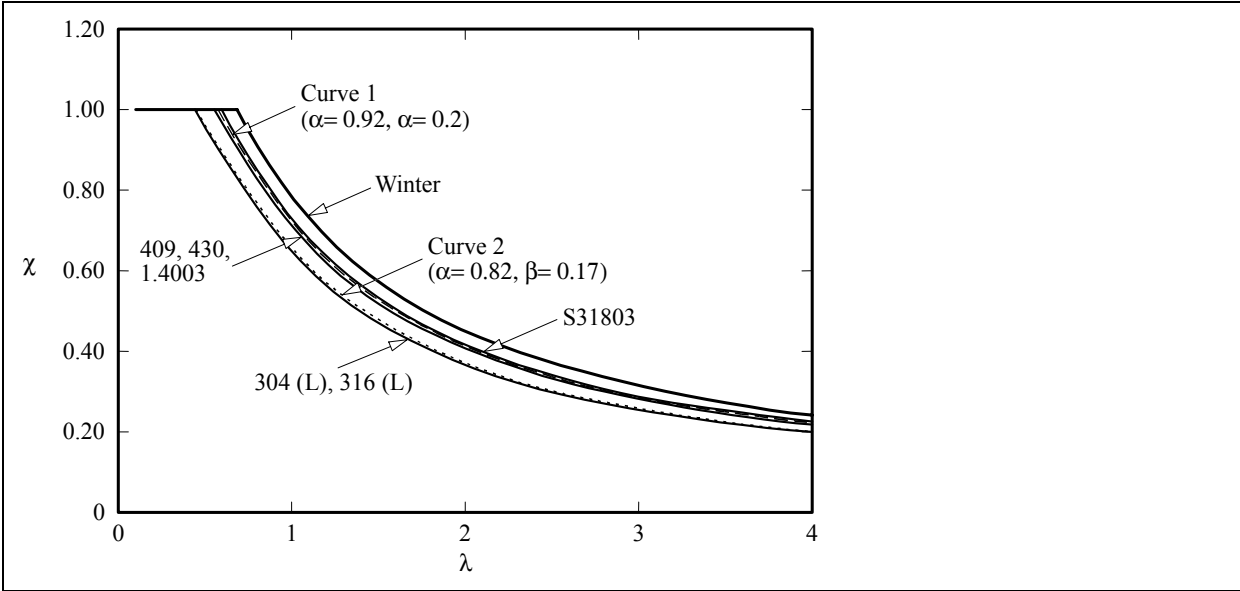


**Figure 8** Strength curves for stiffened plates using the values of  $(E_0, \sigma_{0.2}, n)$  specified in the American and Australian standards

## 6 STRENGTH OF COLD-FORMED SECTIONS WITH STIFFENED ELEMENTS

### 6.1 General

The strength curves defined in Section 5.3 are accurate for single stiffened stainless steel plates. They produce strengths typically 10% less than the Winter strength in the slender range. However, when applied to cold-formed sections, the Winter strength equation is in many cases found to produce more accurate section strengths than those derived in Section 5. The reason for this curious result is to be found in the influence of the corners.

Because of the pronounced capacity to strain-harden, the mechanical properties of stainless steel material can be greatly enhanced when cold-formed into structural shapes. This applies particularly to hollow sections cold-formed from annealed austenitic alloys for which the proof stress values of the flat sides and the corners are typically doubled and tripled respectively compared to the annealed values. It also applies to brake-pressed sections, although in this case the enhanced properties are confined to the corners.

## 6.2 Mechanical properties of cold-formed corners

Gardner [19] showed that the 0.2% proof stress of the corner material ( $\sigma_{c,0.2}$ ) of austenitic cold-formed square and rectangular hollow section tubes may be found with good approximation as,

$$\sigma_{c,0.2} = 0.85\sigma_u \quad (18)$$

where  $\sigma_u$  is the ultimate tensile strength of the flats in the finished cold-formed condition rather than in the coil condition. On the basis of a parametric finite element study, Gardner [19] found that the enhanced corner properties may be extended a width of two times the thickness into the adjacent flats.

For sections brake-pressed from sheet or plate, the 0.2% proof stress of the corner material may be estimated on the basis of research conducted by van den Berg and van der Merwe [20], who produced the following empirical relationship,

$$\sigma_{c,0.2} = \frac{B_c}{(r_i/t)^m} \sigma_{0.2} \quad (19)$$

where  $r_i$  is the internal corner radius and,

$$B_c = 3.289 \frac{\sigma_u}{\sigma_{0.2}} - 0.861 \left( \frac{\sigma_u}{\sigma_{0.2}} \right)^2 - 1.34 \quad (20)$$

$$m = 0.06 \frac{\sigma_u}{\sigma_{0.2}} + 0.031. \quad (21)$$

In equations (19-21), the 0.2% proof stress ( $\sigma_{0.2}$ ) and ultimate tensile strength ( $\sigma_u$ ) pertain to the unformed material.

## 6.3 Design models for the local buckling strength of cold-formed sections

Rasmussen et al. [18] used equations (13-21) to obtain design models that accurately determine the strength of the flat parts and the corners, and compared the models to test strengths for cold-formed tubes [19] and brake-pressed lipped channels [21, 22]. For rectangular tubes with flat widths  $b$  and  $d$ , the following design models were investigated,

$$P_d = 2(\chi_d dt + \chi_b bt) \sigma_{0.2} + A_c \sigma_{0.2} \quad (22)$$

$$P_w = 2(\chi_{d,w} dt + \chi_{b,w} bt) \sigma_{0.2} + A_c \sigma_{0.2} \quad (23)$$

$$P_{d1,ci} = 2(\chi_d dt + \chi_b bt) \sigma_{0.2} + A_c \sigma_c(\epsilon_{\max}) + 8it^2 (\sigma_c(\epsilon_{\max}) - \sigma_{0.2}) \quad (24)$$

$$P_{w1,ci} = 2(\chi_{d,w} dt + \chi_{b,w} bt) \sigma_{0.2} + A_c \sigma_c(\epsilon_{\max}) + 8it^2 (\sigma_c(\epsilon_{\max}) - \sigma_{0.2}) \quad (25)$$

$$P_{d2,ci} = 2(\chi_d dt + \chi_b bt) \sigma_{0.2} + A_c \sigma_{c,0.2} + 8it^2 (\sigma_{c,0.2} - \sigma_{0.2}) \quad (26)$$

$$P_{w2,ci} = 2(\chi_{d,w} dt + \chi_{b,w} bt) \sigma_{0.2} + A_c \sigma_{c,0.2} + 8it^2 (\sigma_{c,0.2} - \sigma_{0.2}) \quad (27)$$

in which  $A_c$  is the area of the corners,  $\epsilon_{\max}$  is the average strain recorded at the maximum load, and  $\sigma_c(\epsilon_{\max})$  is the stress on the corner corresponding to the strain  $\epsilon_{\max}$ , ie. the corner stress attained at the ultimate load. In equations (24-27), the integer  $i$  takes the values 0, 1 and 2 and determines how many times the thickness the corner properties extend into the adjacent flat parts, ie. for  $i=0$  the enhanced corner properties are assumed to be confined to the corner, while for  $i=1$  and  $i=2$ , the enhanced properties are assumed to extend  $t$  and  $2t$  into the adjacent flat parts respectively. The subscripts "b" and "d" refer to the narrow flat width  $b$  and wide flat width  $d$  respectively.

The design strengths  $P_d$  and  $P_w$  defined in eqns (22,23) assume the 0.2% proof stress acts on the effective section (including the corners) in the ultimate limit state.  $P_d$  is based on the strength curve defined by eqn. (13), while  $P_w$  is based on the Winter equation (1) and corresponds to the design strength specified in current American and Australian design standards. The design strengths  $P_{d1,ci}$  and  $P_{w1,ci}$  are similar to  $P_d$

and  $P_W$  except that they assume the corner areas plus a width of  $it$  into each flat element attain the stress  $\sigma_c(\epsilon_{max})$  in the ultimate limit state. The design strength  $P_{d1,ci}$  can be assumed to accurately predict the load supported by the flat elements and the corners, and thus can be expected to lead to the most accurate design strengths. The design strengths  $P_{d2,ci}$  and  $P_{W2,ci}$  are similar to  $P_{d1,ci}$  and  $P_{W1,ci}$  except that they assume the stress on the corner and a width of  $it$  into each flat element is equal to the 0.2% proof stress for the corner ( $\sigma_{c,0.2}$ ).

Gardner [19] presented 31 stub column tests on square hollow section (SHS) and rectangular hollow section (RHS) stainless steel cold-formed tubes, 25 of which were fully effective or nearly fully effective. The remaining six slender tubes were used in [18] for assessing the accuracy of the design strengths defined in eqns (22-27). The tubes were cold-rolled from austenitic 304 material and were *not* stress relieved after forming. Full details of the geometric and material data of the tubes are given in [18, 19]. The specimen labels contained in the first column of Tables 5a,b show the nominal thickness, width and breadth of the tubes. The experimental ultimate strengths are shown as  $P_t$  in Table 5a,b.

**Table 5** Test and design strengths of SHS and RHS stub column tubes [19]

a)  $\sigma_{c,0.2}=\sigma_c(\epsilon_{max})$  on corner regions

Label	$P_t$	$\sigma_c=\sigma_c(\epsilon_{max})$							
		$P_t/P_d$	$P_t/P_W$	Corner only		Corner + $t$		Corner + $2t$	
				$P_t/P_{d1,c0}$	$P_t/P_{W1,c0}$	$P_t/P_{d1,c1}$	$P_t/P_{W1,c1}$	$P_t/P_{d1,c2}$	$P_t/P_{W1,c2}$
(1)	kN	(5)	(6)	(7)	(8)	(9)	(10)	(11)	(12)
SHS100x100x2-SC1	197	1.07	0.97	1.06	0.96	1.04	0.95	1.03	0.94
SHS100x100x2-SC2	187	1.01	0.92	1.01	0.91	1.01	0.91	1.00	0.91
RHS120x80x3-SC1	452	1.08	1.03	1.04	0.99	1.01	0.97	0.99	0.95
RHS120x80x3-SC2	447	1.08	1.03	1.04	0.99	1.01	0.97	0.99	0.95
RHS100x50x2-SC1	182	1.19	1.13	1.13	1.08	1.10	1.05	1.07	1.02
RHS100x50x2-SC2	181	1.19	1.13	1.13	1.08	1.10	1.04	1.06	1.01
Mean		1.10	1.03	1.07	1.00	1.04	0.98	1.02	0.96
St. dev.		0.069	0.084	0.053	0.066	0.043	0.054	0.035	0.044

b)  $\sigma_{c,0.2}=0.85\sigma_u$  on corner regions

Label	$P_t$	$\sigma_{c,0.2}=0.85\sigma_u$							
		$P_t/P_d$	$P_t/P_W$	Corner only		Corner + $t$		Corner + $2t$	
				$P_t/P_{d2,c0}$	$P_t/P_{W2,c0}$	$P_t/P_{d2,c1}$	$P_t/P_{W2,c1}$	$P_t/P_{d2,c2}$	$P_t/P_{W2,c2}$
(1)	kN	(5)	(6)	(13)	(14)	(15)	(16)	(17)	(18)
SHS100x100x2-SC1	197	1.07	0.97	1.03	0.94	1.00	0.91	0.97	0.89
SHS100x100x2-SC2	187	1.01	0.92	0.98	0.89	0.95	0.87	0.92	0.84
RHS120x80x3-SC1	452	1.08	1.03	1.03	0.98	1.00	0.96	0.97	0.93
RHS120x80x3-SC2	447	1.08	1.03	1.02	0.98	0.99	0.95	0.96	0.93
RHS100x50x2-SC1	182	1.19	1.13	1.12	1.07	1.08	1.03	1.04	0.99
RHS100x50x2-SC2	181	1.19	1.13	1.12	1.07	1.08	1.03	1.04	1.00
Mean		1.10	1.03	1.05	0.99	1.02	0.96	0.98	0.93
St. dev.		0.069	0.084	0.057	0.070	0.052	0.065	0.048	0.061

The design strengths defined by eqns (22-27) are compared with the experimental ultimate loads ( $P_t$ ) in Table 5a,b, see [18] for details of the calculation. The following conclusions can be drawn from the comparison:

- The design strength  $P_d$  underestimates the strength of the section, (Column 5 of Table 5a,b). This can be attributed to the conservative modelling of the corners.
- The design strength  $P_W$  (current design approach) overestimates the strength of the specimens SHS100x100x2-SC1 and SHS100x100x2-SC2 but is conservative on an average basis, (Column 6 of Table 5a,b).

- The design strengths  $P_{d1,ci}$ ,  $i=0,1,2$ , are more accurate than  $P_d$ , since the mean of the ratio  $P_i/P_{d1,ci}$  is closer to unity and standard deviation is smaller, (Columns 7, 9 and 11 of Table 5a). The most accurate design strength is  $P_{d1,c2}$  corresponding to a model which assumes the enhanced corner properties extend  $2t$  into the adjacent flat elements. This result is in agreement with Gardner's recommendation for the extent of the corner properties of rectangular tubes. The mean and standard deviation for this model are 1.02 and 0.035 respectively, indicating close agreement between design model and experiment, (Column 11 of Table 5a). However, since the strain  $\epsilon_{\max}$  is generally not known, the model is not suitable for general design purposes.
- The design strength  $P_{W1,ci}$  based on the Winter equation becomes optimistic when the enhanced corner properties are assumed to extend into the flat elements, (Columns 10 and 12 of Table 5a). However, on an average basis, the design strength  $P_{W1,c0}$  matches exactly the tests, (Column 8 of Table 5a).
- The design strength  $P_{d2,ci}$  is in good agreement with the tests when the enhanced corner stress ( $0.85\sigma_u$ ) is assumed to be confined to the corners ( $i=0$ ), (Column 13 of Table 5b). This provides a simple yet accurate design model. The model becomes optimistic when the enhanced corner properties are assumed to extend  $2t$  into the flat elements, (Column 17 of Table 5b).
- The design strength  $P_{W2,ci}$  is optimistic, particularly when the enhanced corner properties are assumed to extend  $2t$  into the flat elements, (Columns 14, 16 and 18 of Table 5b).

The test strengths of specimens RHS100×50×2-SC1 and RHS100×50×2-SC2 are conservatively predicted by all models, (excepting model  $P_{W2,c2}$  which is generally optimistic), and are higher relative to the design strength than the strengths of the other test specimens. It was initially believed that the relatively high design strengths of the RHS100×50×2 sections might have resulted from stresses developing on the fully effective narrow faces which were higher than the assumed design stress ( $\sigma_{0,2}$ ). However, the increase in design load is of the order of 1% when the stress on the narrow face is taken as  $\sigma(\epsilon_{\max})$ , rather than  $\sigma_{0,2}$ , and so this effect does not explain why the otherwise accurate model  $P_{d1,c2}$  produces design strengths that are 6-7% higher than the test strengths for specimens RHS100×50×2-SC1 and RHS100×50×2-SC2. Another possible reason for the relatively high strengths may be that the aspect ratio of the specimens was 0.5 so that the narrow face of the section remained fully effective and may have provided rotational restraint to the wide face. This possibility is explored in Section 6.5

#### 6.4 Effect of enhanced corner properties

Having demonstrated that a) the Winter equation produces optimistic design strengths for stiffened elements and b) the enhanced properties of the corners and possibly rotational restraint from adjacent elements may offset the detrimental effect of gradual yielding, the question arises as to what corner area is required to ensure that the Winter equation can be safely used for the design of sections containing slender stiffened elements. To answer this question, Rasmussen et al. [18] considered the stiffened element shown in Fig. 9 and assumed that half of each adjacent corner is part of the element. The comparison shown in Table 5a,b demonstrated that the design model  $P_{d2,c0}$  is accurate when adjacent elements do not provide significant rotational restraint, and this model was used as the target predictor. For current design provisions based on the Winter equation to be safe, the following requirement must then be met,

$$P_W \leq P_{d2,c0} \Rightarrow p \geq 1 \quad (28)$$

where  $p = P_{d2,c0}/P_W$  is the strength ratio. Assuming  $\lambda > 0.673$ , and substituting eqns (2,5), this ratio can be expressed as,

$$p = \frac{\frac{a}{\lambda} - \frac{\beta}{\lambda^2} + a_c s_c}{\frac{1}{\lambda} - \frac{0.22}{\lambda^2} + a_c} \quad (29)$$

where  $a_c$  and  $s_c$  are the relative corner area and relative corner proof stress respectively, defined as

$$a_c = \frac{A_c}{bt} \quad (30)$$

$$s_c = \frac{\sigma_{c,0.2}}{\sigma_{0.2}} \quad (31)$$

For cold-formed tubes,  $\sigma_{c,0.2}$  may be taken as  $0.85\sigma_u$  (eqn. (18)) where  $\sigma_u$  is the ultimate tensile strength of the flat [19], which may be obtained from eqns (11,12). Accordingly, the ratio  $s_c$  may be obtained as,

$$s_c = \frac{0.85}{0.2 + 185e} \quad (\text{austenitic and duplex alloys}) \quad (32)$$

$$s_c = \frac{0.85 - 0.032(n - 5)}{0.2 + 185e} \quad (\text{ferritic alloys}). \quad (33)$$



**Figure 9** Model of stiffened element

The strength ratio ( $p$ ) is shown in Fig. 10 for groups a, b and c, obtained using the representative values of  $n$  shown in Table 3. The strength ratio is shown for  $a_c = 0, 0.05, 0.1$  and  $0.15$ . These values cover the lower end of the practical range of  $a_c$  varying from about 0.05 to 0.25 for cold-formed tubes. It follows from Fig. 10 that for groups b and c (low strength austenitic alloys and ferritic alloys), the strength ratio is greater than unity for  $a_c \geq 0.1$ , except for a narrow range of small  $\lambda$ -values. Consequently, these groups can be safely designed using the Winter curve provided the corner area exceeds 10% of the flat area. For group a (duplex and high strength austenitic alloys), the strength ratio is greater than unity for  $a_c \geq 0.15$ , (except for a narrow range of  $\lambda$ -values near  $\lambda = 1$  where it is slightly less than unity).

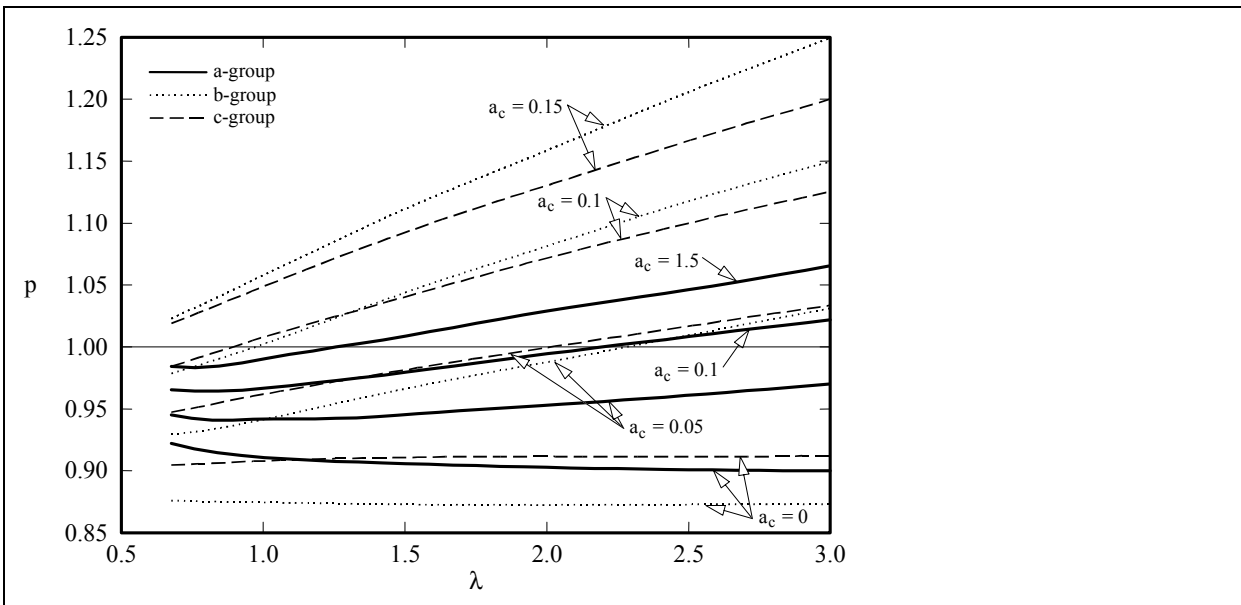


**Figure 10** Graphs of reduction factor ( $p$ ) vs slenderness ( $\lambda$ ) for cold-formed tubes

For  $a_c$ -values less than the limits: 0.15 for group a, and 0.1 for groups b and c, the strength ( $P$ ) of a stiffened element and half of the adjacent corners of a cold-formed tube can be obtained as,

$$P = pP_w \quad (34)$$

where the reduction factor  $p$  can be determined using eqn. (29) or read off Fig. 10, and

$$P_W = (\chi_W bt + A_c) \sigma_{0.2}. \quad (35)$$

For a square hollow section, the strength defined by eqns (34,35) is exactly a quarter of the section strength and there is no restraining effect from adjacent elements. For the SHS100×100×2 section, the reduction factor ( $p$ ) and Winter strength ( $P_W$ ) are obtained as 0.936 and 51.1 kN respectively using eqns (29,34-35). These values lead to a design strength of  $4pP_W = 191\text{kN}$  which is within 3% of the test strengths (187kN and 197kN), thus demonstrating the accuracy of applying eqns (34,35) to slender sections whose stiffened elements are not restrained by adjacent elements.

### 6.5 Effect of restraint from adjacent elements

Figure 11 shows a plot of the ratio of test strength to design strength against aspect ratio ( $D/B$ ). The design models are the  $P_d$ ,  $P_W$ ,  $P_{d1,c2}$  and  $P_{W1,c2}$  models, of which the  $P_{d1,c2}$  model has been shown to be the most accurate. As a general trend, the test to design strength ratio increases with increasing aspect ratio, which could be a result of rotational restraint exerted by the narrow face onto the wide face along the corners. To investigate this possibility, Rasmussen et al. [18] used a rational buckling analysis to accurately determine the plate buckling coefficients of the wide and narrow faces, and calculated the strengths of the component plates on this basis.

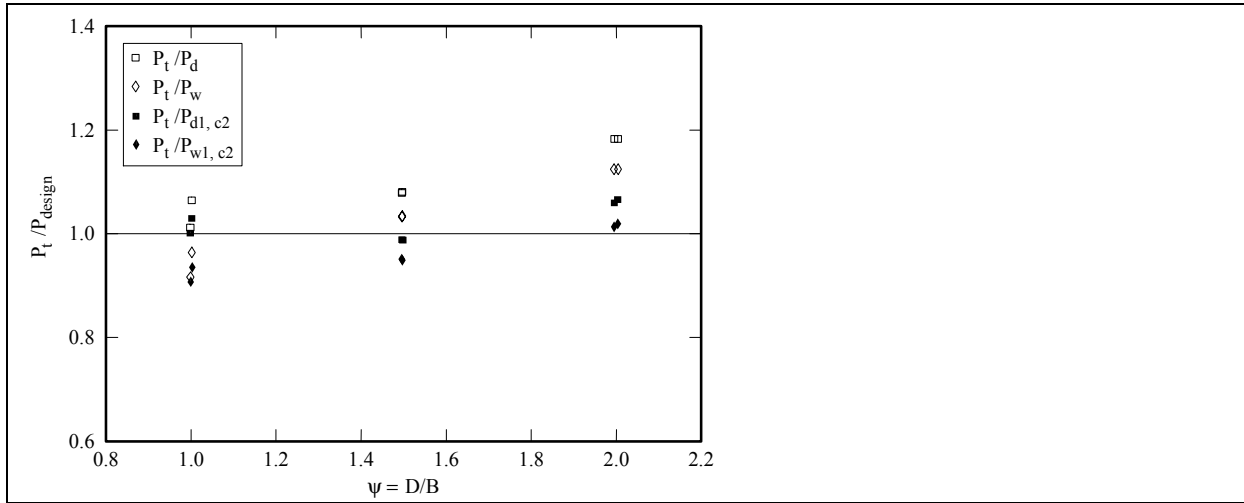


**Figure 11**  $P_{\text{test}}/P_{\text{design}}$  ratios versus aspect ratio ( $\psi$ )

The corners were assumed to be sharp and the plate strength was calculated using the standard Winter equation for simplicity. Accordingly, the design strengths were determined as,

$$P_W^4 = 2(\chi_{d,W}^4 dt + \chi_{b,W}^4 bt) \sigma_{0.2} = (\chi_{d,W}^4 + \chi_{b,W}^4 / \psi) 2dt \sigma_{0.2} \quad (36)$$

$$P_W^k = 2(\chi_{d,W}^k dt + \chi_{b,W}^k bt) \sigma_{0.2} = (\chi_{d,W}^k + \chi_{b,W}^k / \psi) 2dt \sigma_{0.2} \quad (37)$$

$$\psi = \frac{d}{b} \quad (38)$$

where the superscripts '4' and 'k' indicate that the plate buckling coefficient is assumed equal to the classical value of 4 or is calculated from a rational buckling analysis respectively. The results are shown in Fig. 12 as the ratio,

$$p_r = \frac{P_W^k}{P_W^4}. \quad (39)$$

Values of  $p_r$  greater than unity imply that the interaction between component plates increases the design strength. It follows from Fig. 12 that the section strength is increased at small slenderness values, say  $\lambda < 1$ , when based on a rational analysis, and that the increase increases with the aspect ratio. However,

Figure 12 also indicates that at large slenderness values, the design strength is reduced when based on a rational buckling analysis. When applied to Gardner's RHS 120×80×3 ( $\psi=1.5$ ) and RHS 100×50×2 ( $\psi=2$ ) sections, which had plate slenderness values ( $\lambda_d^4$ ) of 0.88 and 1.1 respectively, the strength ratio ( $\rho_r$ ) is 1.005 and 0.984 respectively, suggesting a modest interaction effect for these sections. On the assumption that a rational buckling analysis provides more accurate estimates of strength, interaction effects do not appear to explain the apparent increase in strength with increasing aspect ratio, as observed in Fig 11.

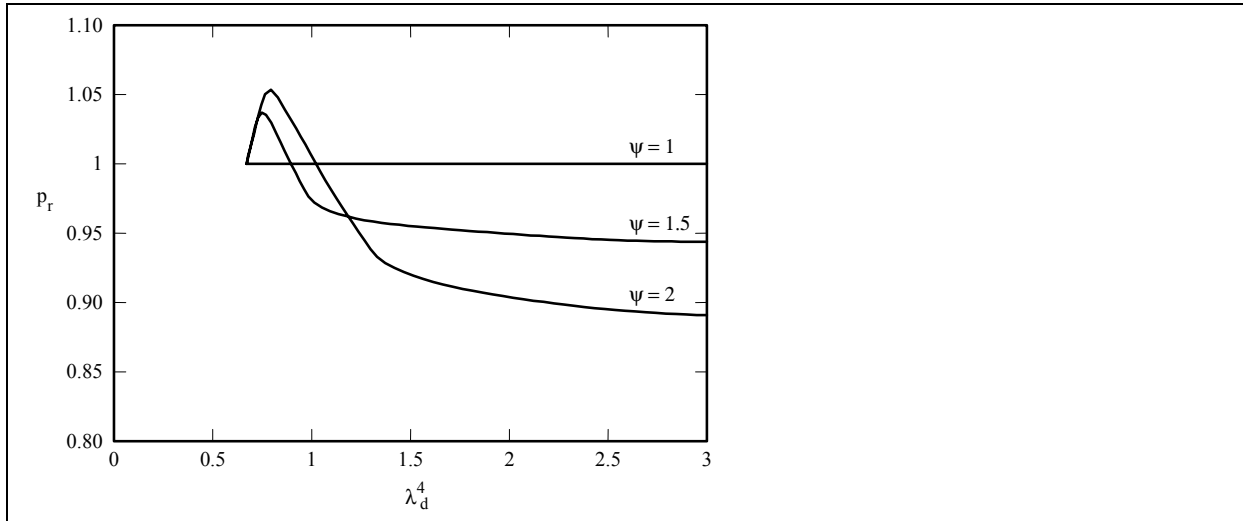


**Figure 12** Comparison of strengths of RHSs based on  $k$ -values determined from a rational buckling analysis relative to strengths based on classical  $k$ -values

### 6.6 Design models for the local buckling strength of brake-pressed sections

Rasmussen et al. [18] also proposed design models for brake-pressed sections in a study similar to that summarised in Sections 6.3 and 6.4 above for cold-formed tubes. The models were compared to tests on lipped channels [21, 22]. As for tubes, the enhanced mechanical properties of the corners proved important and had to be included in the design models to achieve accurate strength predictions. The most accurate design model was  $P_{d1,c0}$  corresponding to using the actual stress on the corner and predicting the plate strength according to the generalised Winter equation. The comparison suggested that for brake-pressed sections, the enhanced corner material is confined to the corner areas.

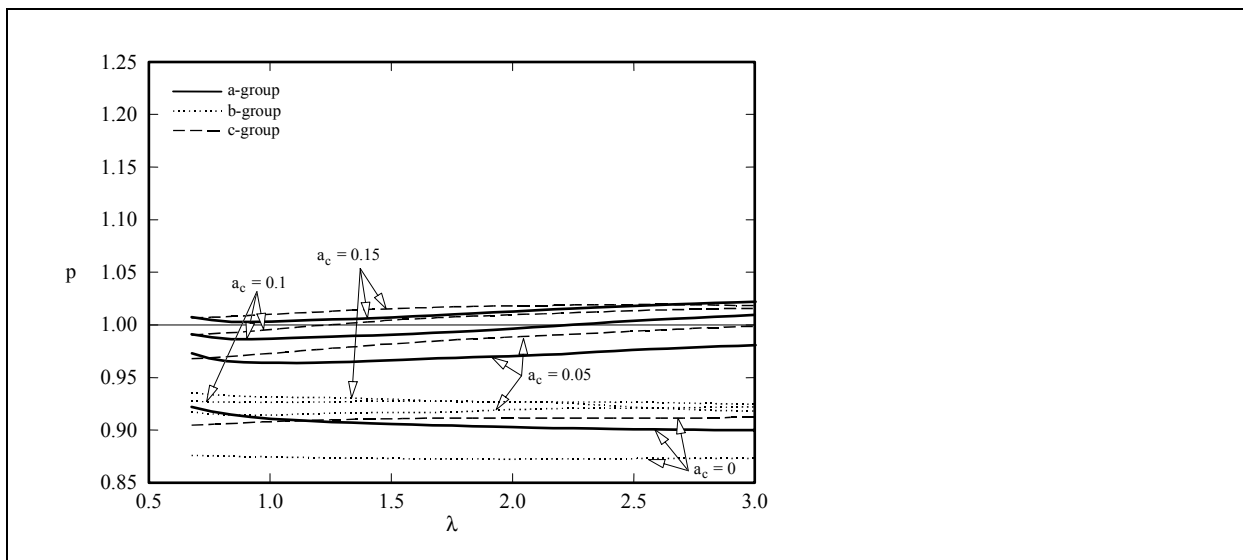


**Figure 13** Graphs of reduction factor ( $\rho$ ) vs slenderness ( $\lambda$ ) for brake-pressed sections

As for slender cold-formed tubes, the reduction factor ( $\rho$ ) to be applied to the Winter strength ( $P_W$ ) in order to produce conservative design strengths can be obtained from eqn. (29). However, for brake-pressed

sections, the ratio ( $s_c = \sigma_{c,0.2}/\sigma_{0.2}$ ) should be determined on the basis of eqns (19-21), rather than eqn. (18) as discussed in [18]. Figure 13 shows graphs of  $p$  vs  $\lambda$  for the values of  $a_c$  of 0, 0.05, 0.1 and 0.15 using the  $(e,n)$ -values representing the a, b and c strength classes defined in Table 3. It follows from Figs 10 and 13 that the reduction factor ( $p$ ) for brake-pressed sections is less sensitive to variations in the nondimensional corner area ( $a_c$ ) and plate slenderness ( $\lambda$ ) than in the case of cold-formed tubes. For strength classes a and c, the maximum reduction in strength below the Winter strength is 3% provided the nondimensional area ( $a_c$ ) is greater than 0.05, which is generally satisfied. For strength class b, the maximum reduction is 8% for  $a_c \geq 0.05$ .

## 7 CONCLUSIONS

The paper summarises research on the local buckling strength of stiffened stainless steel elements. Tests on single plates were used to calibrate accurate finite element models which were used to produce strength curves for a range of mechanical properties defined in terms of  $n$  and  $e = \sigma_{0.2}/E_0$ , where  $n$  is the Ramberg-Osgood exponent. The curves lay below the Winter curve, thus demonstrating that the strength of stainless steel plates is detrimentally affected by gradual yielding.

A generalised Winter equation (13) was used to express the plate strength directly in terms of the parameters  $n$  and  $e$ . Using representative values of  $e$  and  $n$ , several plate strength curves were obtained for the strength classes and cold-worked strength grades defined in Eurocode 3, Part 1.4. The strength curves were close and could be represented by a single curve, which was approximately 10% below the Winter curve. Direct plate strength curves were also obtained for the alloys included in the Australian Standard [7]. In this case, the curves could be represented by two strength curves, both below the Winter curves.

The generalised Winter equation was employed to determine the strength of cold-rolled hollow sections and brake-pressed open sections. However, when applied to such cold-formed sections, the Winter strength equation was in many cases found to produce more accurate section strengths than those based on the generalised Winter equation. The reason for this result was found in the influence of the corners. The mechanical properties of the corners of cold-formed sections are enhanced by the cold-forming process to degrees which in many cases cancel out or exceed the effect of gradual yielding. Consequently, the Winter equation may lead to conservative or optimistic design strengths, depending on the area of the corners relative to the area of the flat parts and the strain-hardening of the corner regions. Furthermore, adjacent elements may be fully effective and provide rotational restraint to the slender stiffened element. These varying and counteracting effects explain why conflicting conclusions are drawn in the literature as to whether the Winter equation can be applied to stainless steel sections without modification, (eg. compare Refs [2] and [8]).

Design models have been proposed which accurately determine the strength of the corner areas and the flat stiffened elements. The models have been verified against tests of slender cold-formed tubes and slender brake-pressed lipped channel sections. The models have been used for determining the minimum corner area required for the Winter equation to safely predict the strength of stiffened elements, and for deriving an expression for the reduction factor to be applied to the Winter strength when the minimum corner area requirement is not met.

It has been shown that the Winter equation leads to conservative strength predictions for stiffened elements provided half of the adjacent corner area exceeds 10 to 15% of the flat area ( $bt$ ), depending on the strength class and whether the section is a cold-rolled tube or a brake-pressed section. A reduction of the Winter strength is necessary when the corner area is less than 10% of the flat area, particularly when the adjacent elements are locally unstable so that they do not provide rotational restraint to the stiffened elements. Uniformly compressed square hollow sections with relatively sharp corners fall in this category of sections.

The effect of interaction between adjacent elements has been investigated for rectangular hollow sections. The interaction was accounted for by determining the plate buckling coefficients for the wide and narrow faces from a rational buckling analysis. It was assumed that the section strength can be more accurately determined by using the actual plate buckling coefficients than the classical value of  $k = 4$ . The results indicated that the section strength is increased at small plate slenderness values but decreased at high

slenderness values when based on a rational buckling analysis. The interaction effect was negligible for the rectangular hollow sections investigated.

While the research has provided evidence supporting the use of the Winter equation for many practical sections, it needs to be borne in mind that the safe use of the Winter equation relies on the enhanced properties of the corners. Consequently, the Winter equation should not be used uncritically for sections which have been annealed after cold-forming, which is often the case for stainless steel tubes. It should also not be used for fabricated sections which do not contain cold-formed corners and are detrimentally affected by welding residual stresses. Furthermore, the Winter equation is likely to produce unsafe predictions for square hollow sections with sharp corners and locally unstable flats.

## 8 REFERENCES

- [1] Bleich, F., *Buckling Strength of Metal Structures*. 1952, New York, NY: McGraw-Hill.
- [2] Johnson, A. and G. Winter, *Behaviour of Stainless Steel Columns and Beams*. Journal of Structural Engineering, American Society of Civil Engineers, ASCE, 1966. **92**(ST5): p. 97-118.
- [3] AISI, *Specification for the Design of Light Gage Cold-formed Stainless Steel Structural Members*. 1968, American Iron and Steel Institute: Washington, DC.
- [4] ASCE, *Specification for the Design of Cold-formed Stainless Steel Structural Members, SEI/ASCE-8*. 2003, American Society of Civil Engineers: New York.
- [5] Stowell, E., *A Unified Theory of Plastic Buckling of Columns and Plates*. 1948, National Advisory Committee for Aeronautics: Washington, DC.
- [6] Wang, S., S. Errera, and G. Winter, *Behaviour of Cold-rolled Stainless Steel Columns*. Journal of Structural Division, American Society of Civil Engineers, ASCE, 1975. **101**, **ST11**: p. 2337-2357.
- [7] AS/NZS4673, *Cold-formed Stainless Steel Structures, AS/NZS4673*. 2001, Standards Australia: Sydney.
- [8] Berg, G.v.d., *The Effect of the Non-linear Stress-strain Behaviour of Stainless Steels on Member Capacity*. Journal of Constructional Steel Research, 2000. **54**(1): p. 135-160.
- [9] Rasmussen, K. and J. Rondal, *Strength Curves for Metal Columns*. Journal of Structural Engineering, American Society of Civil Engineers, 1997. **123**(6): p. 721-728.
- [10] Rasmussen, K. and J. Rondal, *Column Curves for Stainless Steel Alloys*. Journal of Constructional Steel Research, 2000. **54**(1): p. 89-107.
- [11] Rasmussen, K., T. Burns, P. Bezkorovainy and MR Bambach, *Numerical Modelling of Stainless Steel Plates in Compression*. Research Report No. 813, Department of Civil Engineering, University of Sydney, 2002. Available at <http://www.civil.usyd.edu.au/publications/>. Accepted for publication in the Journal of Constructional Steel Research.
- [12] Bambach, M. and K. Rasmussen. *Experimental Techniques for Testing Unstiffened Plates in Compression and Bending*. in *Third International Conference on Thin-walled Structures, Thin-walled Structures - Advances and Developments*. 2001. Cracow, Poland: Elsevier.
- [13] Hill, R., *The Mathematical Theory of Plasticity*. 1950, Oxford: Oxford Science Publications, Clarendon Press.
- [14] Mirambell, E. and E. Real, *On the calculation of deflections in structural stainless steel beams: an experimental and numerical investigation*. Journal of Constructional Steel Research, 2000. **54**(1): p. 109-133.

- [15] Rasmussen, K., *Full-range Stress-strain Curves for Stainless Steel Alloys*. Journal of Constructional Steel Research, 2003. **59**(1): p. 47-61.
- [16] Bezkorovainy, P., T. Burns, and K. Rasmussen, *Strength Curves for Metal Plates*. Research Report No. 821, Department of Civil Engineering, University of Sydney, 2002. Available at <http://www.civil.usyd.edu.au/publications/>. Accepted for publication in the Journal of Structural Engineering, ASCE.
- [17] *Eurocode3: Design of Steel Structures, Part 1.4: Supplementary Rules for Stainless Steel, prENV-93-1-4*. 1996, European Committee for Standardisation: Brussels.
- [18] Rasmussen, K., T. Burns, and P. Bezkorovainy, *Design of Stiffened Elements in Cold-formed Stainless Steel Sections*. Research Report No. 826, Department of Civil Engineering, University of Sydney, 2003. Available at <http://www.civil.usyd.edu.au/publications/>.
- [19] Gardner, L., *A New Approach to Structural Stainless Steel Design*. PhD thesis, Imperial College of Science, Technology and Medicine, London, 2002.
- [20] Berg, G.v.d. and P.v.d. Merwe, *Prediction of Corner Mechanical Properties for Stainless Steel due to Cold Forming*, in *Recent Developments in Cold-formed Steel Design and Construction, 11th International Specialty Conference on Cold-formed Steel Structures*, Eds W-W Yu and R LaBoube, 1992. p. 571-586.
- [21] Kuwamura, H., Y. Inaba, and A. Isozaki. *Local Buckling and Effective Width of Thin-walled Stainless Steel Members*. in *Third International Conference on Thin-walled Structures*. 2001. Krakow, Poland: Elsevier Science Ltd, London.
- [22] Kuwamura, H., Y. Inaba, and A. Isozaki, *Local Buckling and Effective Width of Thin-walled Stainless Steel Members*. 2001, Steel Structural Research Laboratory, Department of Architecture, School of Engineering: Tokyo. (In Japanese).

